NMR study for 4f-localized ferromagnet $CeRu_2Ga_2B$

H. Sakai,* Y. Tokunaga, and S. Kambe
Advanced Science Research Center, Japan Atomic Energy Agency, Tokai, Ibaraki 319-1195, Japan

R. E. Baumbach, F. Ronning, E. D. Bauer, and J. D. Thompson
MPA-CMMS, Los Alamos National Laboratory, Los Alamos, New Mexico 87545, USA
(Received 25 July 2012; published 4 September 2012)

Nuclear magnetic resonance (NMR) studies using ^{11}B and $^{69,71}Ga$ have been performed on the tetragonal Ce-based ferromagnet $CeRu_2Ga_2B$. The Knight shifts for the nuclei show an Ising-type anisotropy along the c axis, similar to results from the static susceptibility. From the Knight shift measurements, the hyperfine coupling constants have been determined. The anisotropy of the spin-lattice relaxation rates $1/T_1$ indicates that the anisotropy of spin fluctuations are also Ising-like along the c axis. The localized character of the 4f electrons in this system is discussed.

DOI: 10.1103/PhysRevB.86.094402 PACS number(s): 75.20.Hr, 75.30.Gw, 75.40.Cx, 75.40.Gb

I. INTRODUCTION

In heavy fermion systems the competition between the Ruderman-Kittel-Kasuya-Yosida (RKKY) exchange interaction and the Kondo effect leads to a rich variety of physical phenomena, such as non-Fermi-liquid behavior, peculiar magnetic ordering, and unconventional superconductivity. The strength of the hybridization between the f and conduction electrons is a key parameter to characterize heavy fermion systems. At the same time, it is very important to understand the anisotropy of the static and dynamic magnetic response, because the strong spin-orbit coupling makes the pseudospins anisotropic. Especially in the antiferromagnetic (AFM) case, systematic NMR studies have revealed that XY-type anisotropy of spin fluctuations correlates with d-wave superconductivity.[1–3] Such a hypothesis is important for developing basic principles to design new materials. It is similarly important to reveal the static/dynamic magnetic anisotropy for ferromagnetic cases. NMR is a powerful tool to microscopically determine the anisotropy of the static/dynamic magnetic response for 4f electrons since the nuclear spins are very low energy probes which allow for the investigation of the electronic responses without strongly perturbing the system. The 4f-electron ferromagnetic (FM) system $CeRu_2Ga_2B$ is suitable for detailed studies of the anisotropy of FM spin fluctuations since there are several NMR-active nuclei (i.e., $^{69,71}Ga$ and ^{11}B).

$CeRu_2Ga_2B$ is a metallic ferromagnet with a Curie temperature $T_C = 16.3$ K.[4] Specific heat measurements suggest that the FM transition is weakly first order and, additionally, that the Ce 4f-electron states do not hybridize strongly with the conduction electron states, that is, the 4f electrons are well localized. The isomorphic $CeRu_2Al_2B$ is also a ferromagnet with $T_C = 12.8$ K, but it additionally exhibits antiferromagnetism just above T_C ($T_N = 14.2$ K).[5,6] Such complex magnetic behavior indicates a competition between FM and AFM exchange interactions in $CeRu_2Al_2B$. Very recently, an NMR study of $CeRu_2Al_2B$ revealed that the Ising-type magnetic anisotropy comes from the $\Gamma_7^{(1)}$ doublet ground state, that is, a nearly pure $|J_z\rangle = |\pm 5/2\rangle$ state arises due to crystal electric field (CEF) effects.[7] Each CEF level is well separated in energy, where the first excited CEF state $\Gamma_6 = |\pm 1/2\rangle$ is proposed to lie at ~550 K above the ground state. In both compounds, T_C increases under applied pressures up to about 2.6 GPa, while the T_N decreases and finally disappears for $CeRu_2Al_2B$.[8] To reach the possible FM quantum critical region, further pressure or alternative chemical substitutions are required.

The crystal structure for $CeRu_2Ga_2B$ is displayed in Fig. 1. It is expressed as a stuffed version of the tetragonal $CeMg_2Si_2$ structure with the space group $P4/mmm$.[9] In this layered structure, the Ce atoms form a square lattice in the Ce layer and the Ru and B atoms form nesting square lattices. The Ga layers are sandwiched between the Ce and Ru-B layers, which are stacked alternately along the c direction. The lattice parameters for $CeRu_2Ga_2B$ are $a = 4.187$ Å and $c = 5.580$ Å, respectively.[4] Such a layered tetragonal crystal structure often gives a versatile template, as is seen for the tetragonal $ThCr_2Si_2$- and $HoCoGa_5$-type structures. Indeed, the isostructural compounds $LnRu_2X_2X'$ (Ln = La, Ce, Pr, Nd, Sm; X = Al, Ga; X' = B, C) are already reported,[5,6,8,9] and show a variety of magnetic properties. Systematic investigations on those compounds may provide a route to explore new heavy fermion systems. It is noted that the ratio $c/a \sim 1.3$ for $CeRu_2Ga_2B$ is not large when compared with the typical values of ~2.4 for the heavy fermion superconductors $CeCu_2Si_2$ ($ThCr_2Si_2$ type)[10] and ~1.6 for $CeCoIn_5$ ($HoCoGa_5$ type).[11]

In this paper, ^{11}B and $^{69,71}Ga$-NMR measurements for $CeRu_2Ga_2B$ are reported using both single crystal and polycrystalline specimens. First, the NMR spectra under applied fields are shown, then the hyperfine coupling constants for $^{69,71}Ga$ and ^{11}B are determined via Knight shifts in the paramagnetic state under applied fields. The nuclear quadrupolar parameters are also obtained, which reflect the electric field gradients (EFGs) on the subjective nuclear sites. Second, the NMR spectra under zero applied field are shown in order to determine the internal fields on the nuclear sites. Finally, we discuss the dynamic magnetic response of 4f electrons in this system via nuclear spin-lattice relaxation rates ($1/T_1$) measurements.

II. EXPERIMENT

Polycrystalline specimens of $CeRu_2Ga_2B$ were synthesized by arc melting stoichiometric quantities of Ce, Ru, Ga, and B under an Ar atmosphere. The resulting boules were flipped and remelted several times to encourage homogeneity and

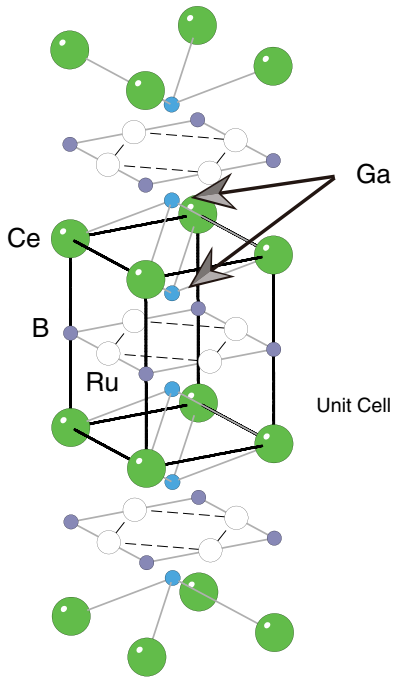

FIG. 1. (Color online) Crystal structure of $CeRu_2Ga_2B$.

subsequently were annealed at 900 °C for two weeks in evacuated quartz tubes. These specimens were checked by x-ray diffraction (XRD) measurements to confirm the single phase without any secondary phases. The resulting XRD patterns indicated a phase-pure $LaRu_2Al_2B$ structure, and the obtained lattice parameters were in good agreement with previously reported values. Single crystals for $CeRu_2Ga_2B$ were grown by the Czochralski pulling method.[4]

Magnetization was measured using a SQUID magnetometer (Quantum Design Magnetic Property Measurement System) with applied fields of 1 kOe along the a and c axes of the single crystal. Magnetic susceptibility (χ) below T_C is defined as the magnetization (M) divided by the applied field (H_0), that is, $\chi \equiv M/H_0$.

NMR measurements were carried out using a phase-coherent, pulsed spectrometer. Frequency-swept spectra were taken by tuning the rf network at each point. To form the nuclear spin echoes, 90°–180° conditions were used with a first pulse duration of 2–3 μs. The separation τ between first and second pulses was typically 10–20 μs. External magnetic fields were applied using a homogeneous superconducting magnet specified for NMR. In the paramagnetic state, a single crystal with dimensions of $0.6 \times 0.6 \times 5$ mm^3 was used for the NMR measurements. In the FM ordered state, the zero applied field NMR measurements were performed using the polycrystalline sample. Using the internal fields on the active nuclei, the NMR spectra were taken by sweeping the frequency.

Using conventional notation, the quadrupole frequency parameter is defined as $\nu_Q \equiv \frac{3e^2qQ}{2I(2I-1)h}$, where eQ is the nuclear quadrupolar moment, I is the nuclear spin quantum number, and $eq \equiv V_{ZZ}$ is the principal component of the electric field gradient (EFG) tensor. Here V_{ii} denotes EFG tensor components in the principal coordinate system, such that $|V_{XX}| \leqslant |V_{YY}| \leqslant |V_{ZZ}|$ for each ionic site. The EFG components satisfy LaPlace's equation, that is, $V_{XX} + V_{YY} + V_{ZZ} = 0$. The EFG asymmetry parameter is defined as $\eta \equiv \frac{|V_{YY}-V_{XX}|}{|V_{ZZ}|}$. At the tetragonal sites, η becomes 0. Nuclear quadrupolar moments are $^{11}Q = 0.0355 \times 10^{-24}$ cm^2, $^{69}Q = 0.178 \times 10^{-24}$ cm^2, and $^{71}Q = 0.112 \times 10^{-24}$ cm^2, respectively. Nuclear gyromagnetic ratio values used here are $^{11}\gamma_N/2\pi = 1.366$ MHz/kOe, $^{69}\gamma_N/2\pi = 1.022$ MHz/kOe, and $^{71}\gamma_N/2\pi = 1.29855$ MHz/kOe.

The nuclear spin-lattice relaxation time T_1 was measured using the inversion-recovery method with a π pulse. Values of T_1 were obtained from fits to an appropriate relaxation function. The magnetization recovery $[\{M(\infty) - M(t)\}/M(\infty)]$ for the center and satellite NMR lines of the ^{11}B and ^{69,71}Ga ($I = 3/2$) nuclei gave satisfactory fits to the single-T_1 functions $0.1\exp(-t/T_1) + 0.9\exp(-6t/T_1)$ and $0.1\exp(-t/T_1) + 0.5\exp(-3t/T_1) + 0.4\exp(-6t/T_1)$, respectively.

III. RESULTS AND DISCUSSIONS

A. Static magnetic response

Figure 2(a) shows the frequency-swept NMR spectra taken at 80 K under a constant field of ~72 kOe along the c axis of a single crystal. In this case, the observed NMR lines are successfully assigned as shown in Fig. 2(a). On the other hand, the NMR for ^{69,71}Ga with $H_0 \parallel a$ could not be observed, as

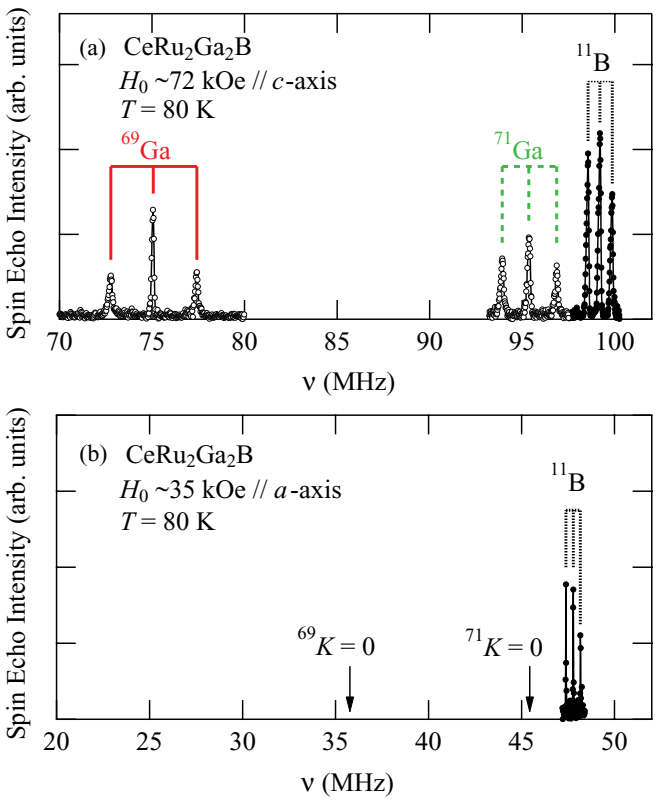

FIG. 2. (Color online) Frequency-swept NMR spectra taken at 80 K for the single crystal of $CeRu_2Ga_2B$ (a) under an external field of $H_0 \sim 72$ kOe along the c axis, and (b) under an external field of $H_0 \sim 35$ kOe along the a axis.

shown in Fig. 2(b), even under the higher field of ∼72 kOe (not shown). The reason why the ^{69,71}Ga NMR signals are not observed may be due to the fast nuclear spin-spin relaxation rates $1/T_2$ and not due to $1/T_1$, as discussed later.

Each set of spectra for ^{11}B and ^{69,71}Ga should be composed of three equally separated lines, that is, one center ($1/2 \leftrightarrow -1/2$) and two satellite ($-1/2 \leftrightarrow -3/2$ and $3/2 \leftrightarrow 1/2$) transitions since all the nuclear spins are $I = 3/2$ and all the nuclear sites have tetragonal symmetry ($\eta = 0$). Within first order perturbation of the nuclear quadrupolar interaction, in the case of $H_0 \parallel V_{ZZ}$, the resonance frequency for the transition of $m \leftrightarrow m-1$ is described as $\nu_m = \nu_0(1+K_c) + \nu_Q(m-1/2)$, while in the case of $H_0 \perp V_{ZZ}$, $\nu_m = \nu_0(1+K_a) - (\nu_Q/2)(m-1/2)$ with $\nu_0 \equiv \gamma_N H_0$. While the second order perturbation gives a frequency shift of $\frac{3\nu_Q^2}{16\nu_0}$ for the central transition in the case of $H_0 \perp V_{ZZ}$, the separations between the satellite lines are independent of a second order perturbation effect, that is, $2\nu_Q$ and ν_Q in the case of $H_0 \parallel$ and $\perp V_{ZZ}$, respectively. The center line for the case of $H_0 \parallel V_{ZZ}$ is also free from any second order perturbation.

From the site symmetry and magnetic anisotropy along the c axis, the principal axes for V_{ZZ} are determined to be along the c axis for both ^{11}B and ^{69,71}Ga. Indeed, in the case of $H_0 \parallel c$, the separations between satellite lines for ^{11}B are doubled, as compared to $H \parallel a$ as shown in Fig. 2(b). It is noted that the direction of V_{ZZ} for ^{69,71}Ga is additionally confirmed by the NMR measurement under zero applied field, as described later. Since the ν_Q are much less than the experimental ν_0 in the case of $H_0 \sim 72$ kOe, as mentioned above, the second order perturbation is enough to be taken into account. The obtained ratio of $^{69,71}\nu_Q$ accurately corresponds to the ratio of the nuclear quadrupolar moment $^{69,71}Q$. In addition, the ratio of the central resonance frequencies for ^{69,71}Ga also corresponds to the ratio of $^{69,71}\gamma_N$.

The nuclear quadrupolar frequencies ν_Q for each nucleus are estimated from the separation between satellite lines. The ν_Q for ^{11}B and ^{69}Ga are plotted against temperature in Fig. 3, in which the results obtained in the FM ordered state under zero applied field are also plotted together as described below. The error bars in Fig. 3 are roughly estimated as a maximum error assuming ±10° misalignment of the crystal relative to the external field. Although a small variation just below T_C is seen for ^{69}Ga, ν_Q is estimated to be ∼0.7 MHz for ^{11}B and ∼2.4 MHz for ^{69}Ga in the paramagnetic state. The ν_Q for ^{11}B was not estimated in the ordered state since the NMR frequencies were lower than the experimental frequency range under zero applied field.

Here ν_Q for ^{11}B in $CeRu_2Ga_2B$ is similar to the experimental value of 0.75 MHz in isostructural $CeRu_2Al_2B$. The calculation of ν_Q based on a full potential linear augmented plane wave (FLAPW) method within the local density approximation (LDA) assuming itinerant 4f electrons[7] has found similar values for ^{11}B in $CeRu_2Al_2B$ (0.78 MHz) and $LaRu_2Al_2B$ (0.73 MHz). These nearly independent values for ^{11}B from $CeRu_2Ga_2B$ and $LaRu_2Al_2B$ suggest that the Ce 4f electrons hardly contribute to the EFG on the B sites with very low hybridization with B 2p electrons, even if 4f itinerancy is assumed. The EFG V_{ZZ} on the B sites is $\sim 1.4 \times 10^{17}$ V/cm^2. In the case of the Ga sites, the $^{69}\nu_Q$ yields $V_{ZZ} \approx 1.0 \times 10^{17}$ V/cm^2. The EFGs on the B and Ga sites are very similar.

Next, the static magnetic response to an applied field $H_0(\boldsymbol{q} = 0, \omega = 0)$ for $CeRu_2Ga_2B$ is shown. The bulk magnetic susceptibility $\chi(\boldsymbol{q} = 0, \omega = 0) \equiv \chi(0,0)$ along the a and c axes shows Curie-Weiss behavior in the paramagnetic state, as shown in Fig. 4. The Curie temperature T_C in zero external field is estimated to be 16.3 K from specific heat measurements,[4] which corresponds to a sudden increase of M below ∼20 K in Fig. 4. T_C rapidly broadens and slightly increases under an applied magnetic field, as expected for a ferromagnet. In this temperature region, χ is strongly suppressed by applied field. The magnetic susceptibility along the c axis is much larger than that along the a axis below ∼200 K. In the ordered state below T_C, the magnetic anisotropy is uniaxial along the c axis. Curie-Weiss fits for the a and c axes data above 300 K lead to effective moments μ_{eff} of ∼1.0 μ_B/Ce and ∼1.8 μ_B/Ce and the Weiss temperatures Θ of positive ∼45 K and negative ∼34 K, respectively. The temperature-independent term is fitted to be $\chi_0 \sim 0.001$ emu/mol for both axes. The reduced effective moment from the free-ion Ce^{3+} value of 2.54 μ_B is suggested to originate

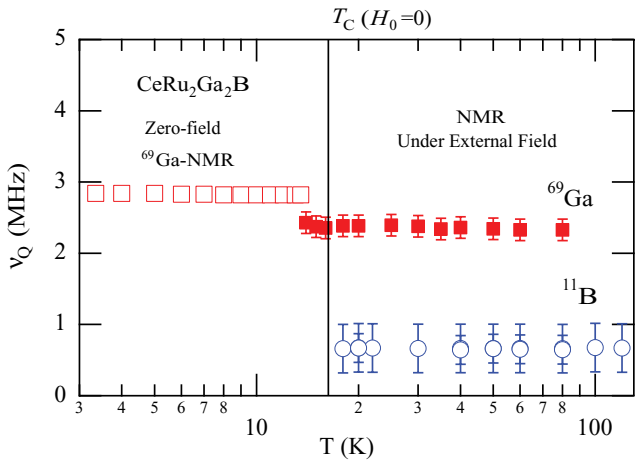

FIG. 3. (Color online) Temperature dependence of the nuclear quadrupolar frequency ν_Q for ^{11}B and ^{69}Ga.

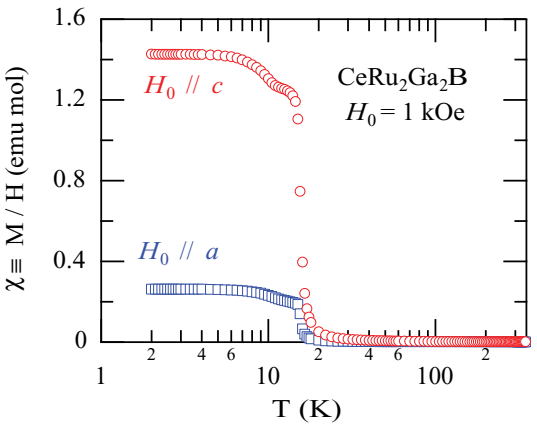

FIG. 4. (Color online) Temperature dependence of magnetic susceptibility $\chi \equiv M/H_0$ for a single crystal of $CeRu_2Ga_2B$ measured at $H_0 = 1$ kOe. The T axis is logarithmic.

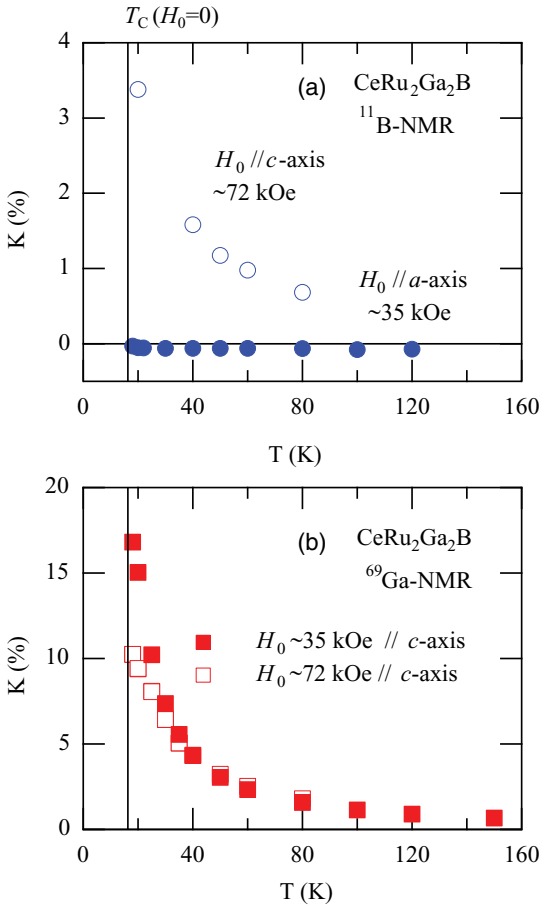

FIG. 5. (Color online) Temperature dependence of Knight shifts for (a) ^{11}B and (b) ^{69}Ga in $CeRu_2Ga_2B$.

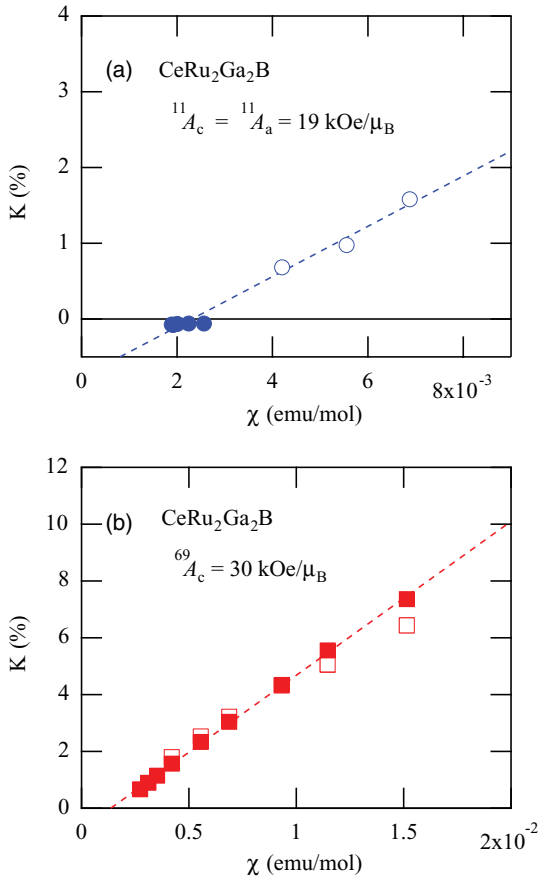

FIG. 6. (Color online) K-χ plots for (a) ^{11}B and (b) ^{69}Ga in $CeRu_2Ga_2B$. The symbols are the same as in Fig. 5.

from the CEF effect, not due to hybridization.[7] The sign change of Θ may suggest a competition between FM and AFM interactions. From the magnetization curve at 2 K up to 50 kOe using the polycrystalline sample, the saturated moment is roughly 1.25 μ_B/Ce and the coercive magnetic force is very small, less than 0.2 kOe.[4] Probably the upturn in the static χ_a below ~30 K may come from a small misalignment of the crystal relative to the external field since the Knight shift for ^{11}B-NMR corresponding to the χ_a is nearly temperature independent, as shown below.

In Fig. 5 the temperature dependence of the Knight shift for ^{11}B and ^{69}Ga is shown, which are determined from the center NMR lines. In general, the Knight shift K reflects the local magnetic susceptibility on the nucleus due to the static field H_0, that is, $K = A_{hf}\chi(0,0) \propto H_{local}$, where A_{hf} is the hyperfine coupling constant. As seen in K for ^{69}Ga along the c direction, K is field dependent below ~30 K, similar to $\chi(0,0)$, that is, $^{69}K_c$ in this temperature range is strongly suppressed by an applied field. Although $^{69}K_a$ could not be determined, K for ^{11}B shows an Ising-type anisotropy along the c axis, which is similar to the static $\chi(0,0)$. $^{11}K_a$ is nearly zero and almost temperature independent, as noted already.

The Knight shifts for ^{11}B and ^{69}Ga are plotted against the static susceptibility χ, with temperature as an implicit parameter, to derive the hyperfine coupling constants, that is, the so-called K-χ plot as shown in Fig. 6. Since K and χ are field dependent below ~30 K, a bending of K-χ is seen near ~30 K. Here the data above 30 K are plotted. Above ~30 K, the K-χ plots show a linear relationship which gives the hyperfine coupling constants $^{11}A_{a,c} = 19$ kOe/μ_B and $^{69}A_c = 30$ kOe/μ_B. The classical dipolar hyperfine coupling constants can be estimated to be at most ~0.3 kOe/μ_B for the Ga sites and ~2 kOe/μ_B for the B sites. Since these values are much smaller than the experimental values, the transferred hyperfine fields are mainly caused by RKKY-type oscillations through conduction electrons from Ce 4f moments. As for ^{11}A, since the K_a and χ_a are located on an extension of the K_c vs χ_c line as shown in Fig. 6(a), it is reasonable to assume that the coupling constant is isotropic. Therefore, anisotropy in the spin-lattice relaxation rates $1/T_1$, as shown later, cannot be explained by an anisotropy in hyperfine coupling constants.

B. Zero-field NMR measurement

In ferromagnets, using the internal fields transferred on the nuclei, zero-field NMR measurement are possible at temperatures well below T_C. As shown in Fig. 7, the frequency-swept NMR spectra at 3.3 K under zero applied field are successfully obtained for $CeRu_2Ga_2B$. Each line is quite narrow, with a width about 100 kHz, which reflects the good sample quality. It is noted that no NMR lines were observed in the frequency range 16 to ~35 MHz. The NMR signal under

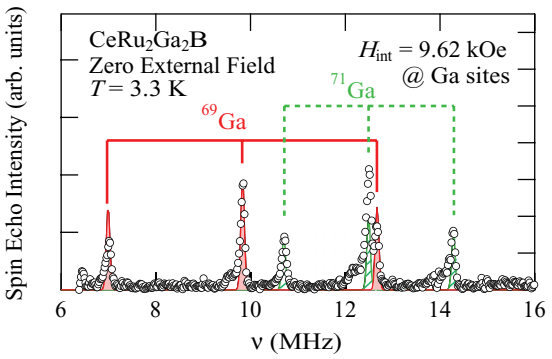

FIG. 7. (Color online) Zero applied field NMR spectra taken at 3.3 K. The site assignments for the observed lines are indicated. The solid curves and hatched Lorentzians are drawn based on a simulation with the natural width of 100 kHz.

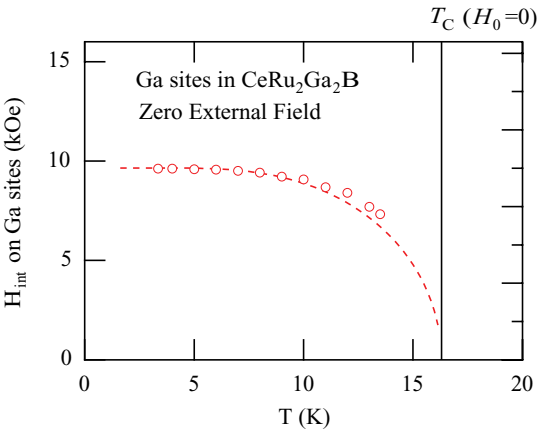

FIG. 8. (Color online) Temperature dependence of the transferred internal field on the Ga sites. The dotted curve is a guide to eyes.

zero field is observable up to ∼13.5 K. The signal above 14 K cannot be detected because the relaxation rates become shorter.

In this frequency range, six NMR lines are observed, which are successfully assigned to ^{69,71}Ga as indicated in Fig. 7. The spectra can be explained by the internal field $H_{\rm int}$ on the Ga sites parallel to the c axis. The $\nu_{\rm Q}$ and $H_{\rm int}$ are estimated by numerical diagonalization of the Hamiltonian matrix, including Zeeman ($\gamma_{\rm N}\boldsymbol{H}_{\rm int}$) and quadrupolar terms. The assignment is fully validated by the ratio of central frequencies for ^{69,71}Ga corresponding to the ratio of gyromagnetic ratios $\gamma_{\rm N}$ and the ratio of the width between satellite frequencies corresponding to the ratios of quadrupolar moment Q.

In ferromagnets, rf fields (H_1) for the nuclear spin excitation are effectively enhanced due to the electronic spin oscillations which give an enhancement factor of ∼10–100 and/or due to FM domain wall motion which gives a factor of 10^3–10^4 to the "bare" H_1. This is the so-called H_1 enhancement. In the ligand NMR, the former enhancement by on-site electronic oscillations would be small. Indeed, in the present case, the H_1 enhancement is not so large (it is less than a factor of 10, at most) as compared with the pulse conditions in paramagnetic materials. The FM softness with low coercive magnetic force and the good purity without domain wall pinning by impurities are also known to reduce the enhancement factor by domain wall motions.

The obtained $\nu_{\rm Q}$ values of ∼2.8 MHz in the ordered state are plotted in Fig. 3 and are a bit larger than the estimate of ∼2.4 MHz in the paramagnetic state, even if errors due to misalignment are considered in the case of NMR under applied fields. A small change of EFG may result from a lattice expansion below $T_{\rm C}$, which could occur if the FM phase transition is first order, although the local site symmetry on Ga sites remains tetragonal through $T_{\rm C}$ according to the NMR spectra. It may be interesting to determine the volume change by thermal expansion measurements.

The estimated internal field $H_{\rm int}$ from $\nu_{\rm res}/\gamma_{\rm N}$ is plotted against temperature in Fig. 8. Below ∼8 K, $H_{\rm int}$ is almost saturated to 9.6 kOe. Again, it cannot be explained by the classical dipolar fields from Ce ions with about 1 $\mu_{\rm B}$. The hyperfine mechanism should be due to the RKKY interaction through the conduction electrons, meaning that it would be predominantly isotropic. If we adopt the hyperfine coupling constant obtained in the paramagnetic state, the ordered moment can be estimated to be 1.3 $\mu_{\rm B}$/Ce with the hyperfine coupling constant $^{69}A'_c = {}^{69}A_c/4$ divided by the number of nearest-neighboring Ce ions from the Ga sites. This estimate of the ordered moment is in good agreement with the saturation moment in magnetization measurements.[4] Thus, in the ordered state, the NMR spectra can be well understood by localized moments on Ce ions.

In the ordered state below $T_{\rm C}$, there is no additional anomaly in the temperature dependence of $H_{\rm int}$ and $\nu_{\rm Q}$, although a small anomaly around 6 K in specific heat and magnetization measurements[4] is reported. The origin of the 6 K anomaly is not clear.

C. Dynamic magnetic response

To deduce the dynamic magnetism, the nuclear spin-lattice relaxation rates $1/T_1$ are measured on the ^{69}Ga sites under applied fields of ∼35 and ∼72 kOe, and under zero applied field. Figure 9(a) shows the temperature dependence of $1/T_1$ for ^{69}Ga. In the paramagnetic state, $1/T_1$ for ^{11}B is also measured as shown in Fig. 9(b).

Above $T_{\rm C}$, as seen in $1/^{69}T_1$, an external field suppresses $1/T_1$ significantly in the temperature region below ∼40 K. This means that an applied field quickly quenches the low-energy spin fluctuations in the FM enhanced susceptibility around $\boldsymbol{q} = 0$. Such a suppression of $1/T_1$ has been widely observed in FM materials. Thus, the dynamical susceptibility is ferromagnetically enhanced below ∼40 K. Above ∼40 K, $1/T_1$ becomes rather field independent. Interestingly, $1/^{11,69}T_1$ decreases above ∼40 K as temperature increases. Typically in the localized case of 4f electrons, only fluctuations by the intersite exchange interaction $J_{\rm ex}$ govern the T_1 process, and $1/T_1$ becomes temperature independent. Such a decrease of $1/T_1$ in the high temperature region should originate partly from the relaxation dominated by intrasite exchange $J_{\rm cf}$ via conduction electrons.

In general, NMR $1/T_1$ can be expressed[12] as

$$\frac{1}{T_1} = \frac{k_{\rm B}T}{(\gamma_{\rm e}\hbar)^2} 2(\gamma_{\rm N}A_\perp)^2 \sum_{\boldsymbol{q}} f_\perp^2(\boldsymbol{q}) \frac{{\rm Im}\chi_\perp(\boldsymbol{q},\omega_0)}{\omega_0}, \qquad (1)$$

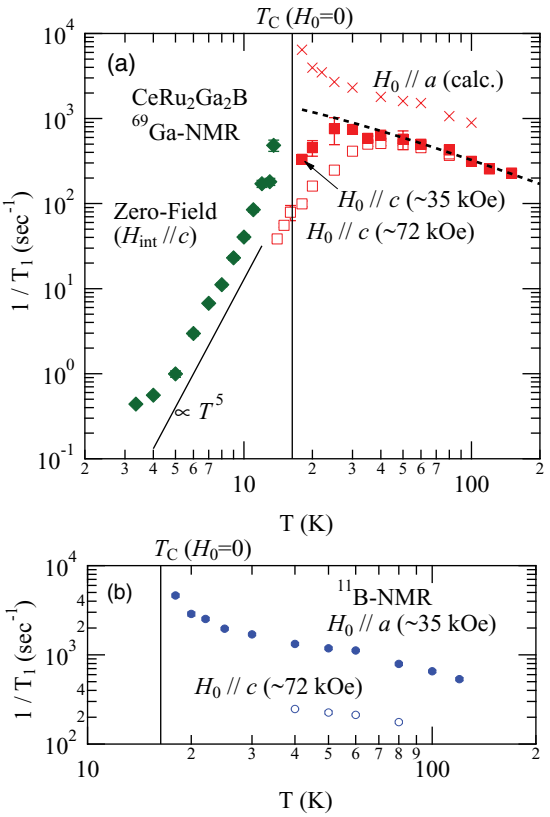

FIG. 9. (Color online) (a) Temperature dependence of the nuclear spin-lattice relaxation rates $1/T_1$ for ^{69}Ga, and (b) for ^{11}B in $CeRu_2Ga_2B$. The dotted curve is a guide to eyes for extrapolation of $1/T_1$ in zero field. The cross marks (×) indicate the estimates for ^{69}Ga in the case of $H_0 \parallel a$ from the observed values for ^{11}B.

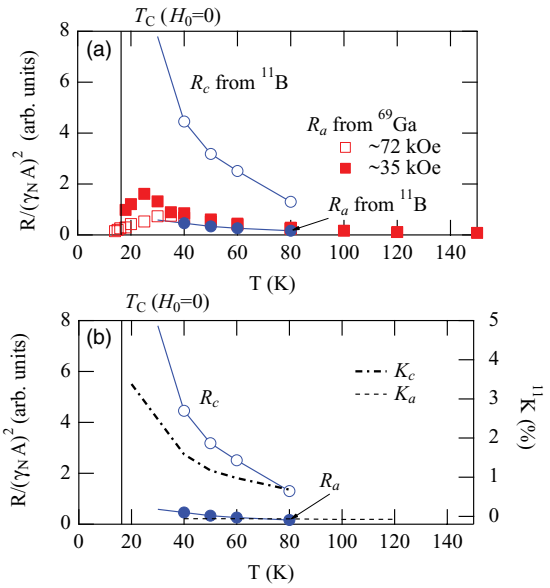

FIG. 10. (Color online) (a) The temperature dependence of deduced $R_i/(\gamma_N A_i)^2$ $(i = a, c)$ for ^{11}B and $R_a/(\gamma_N A_a)^2$ for ^{69}Ga corresponding to the $\boldsymbol{q}$-summed imaginary part of dynamical susceptibility for the quantization i axis. See text for the detailed definition of R_i. (b) A comparison of anisotropy for R_i with the Knight shifts for ^{11}B corresponding to the static susceptibility χ.

where γ_e is the electronic gyromagnetic ratio, $f_\alpha(\boldsymbol{q})$ is the hyperfine form factor, $\mathrm{Im}\chi(\boldsymbol{q},\omega_0)$ is the imaginary part of dynamical susceptibility, ω_0 is the nuclear Larmor frequency, and the suffix $\perp$ refers to the component perpendicular to the quantization axis. In this case, since the principal mode of spin fluctuations is FM $(\boldsymbol{q} = 0)$, $f(q)$ can be set to unity for simplicity. The corresponding $1/T_1$ for ^{71}Ga in the paramagnetic state (not shown) is larger by a factor of γ_N^2. Thus, the relaxation mechanism is confirmed to be magnetic and the uniform dynamical susceptibility of $4f$ electrons governs the T_1 process.

To discuss the anisotropy of the dynamical susceptibility, a new rate R_i along the quantization i axis is defined as $R_i \equiv k(\gamma_N A_i)^2 \sum_{\boldsymbol{q}} \mathrm{Im}\chi_i(\boldsymbol{q},\omega_0)/\omega_0$ $(i = a, c)$ with a numerical constant k of $k_B/(\gamma_e\hbar)^2$. Then, from Eq. (1), $(1/T_1T)_{H_0\parallel c} = 2R_a$ and $(1/T_1T)_{H_0\parallel a} = R_a + R_c$ are given. In this way, the R_i divided by $(\gamma_N A_i)^2$ corresponding to the $\sum_{\boldsymbol{q}} \mathrm{Im}\chi_i(\boldsymbol{q},\omega)$ are decomposed from the anisotropy in $1/T_1$, as shown in Fig. 10. Here A_a for ^{69}Ga is assumed again to be $A_a = A_c$. Since $R_a/(\gamma_N A_a)^2$ from ^{69}Ga NMR is in good agreement with that from ^{11}B NMR, this assumption is justified. As shown in Fig. 10, $\sum_{\boldsymbol{q}} \mathrm{Im}\chi_c(\boldsymbol{q},\omega)$ is much larger than $\sum_{\boldsymbol{q}} \mathrm{Im}\chi_a(\boldsymbol{q},\omega)$, that is, the c-axis spin fluctuations are dominant in $CeRu_2Ga_2B$ and the $4f$ electron pseudospin also fluctuates with an Ising-type magnetic anisotropy even in the paramagnetic state. A comparison of R_i with the Knight shifts for ^{11}B is shown in Fig. 10(b). In the case of an itinerant FM, $\sum_{\boldsymbol{q}} \mathrm{Im}\chi(\boldsymbol{q},\omega)$ should be simply proportional to the static susceptibility $\chi(0,0) \propto K$.[13] For example, such a scaling between χ and R_i is seen in itinerant FM systems (e.g., UCoGe).[14] As shown in Fig. 10(b), however, this is clearly not the case for $CeRu_2Ga_2B$ since the R_i do not scale with K_i.

With the obtained R_a and R_c from ^{11}B NMR, the unobservable $1/T_1$ along the a axis for ^{69}Ga can be estimated, as plotted in Fig. 9. These $1/T_1$ values do not exceed the NMR observable limit, which is roughly 10^4 s^{-1}. Therefore, the main reason why the signal of ^{69}Ga is missed in the case of $H_0 \parallel a$ is that the spin-spin relaxation rate $1/T_2$ is too fast, that is, a much shorter separation τ may be required but is experimentally limited.

In the high temperature region above ~40 K (well above T_C), the nuclear-spin relaxation can be regarded as being driven by fluctuations of the Ce local moments. In the simplified model for localized $4f$ electrons, assuming the isotropic hyperfine coupling A_{iso} and $\boldsymbol{q}$-independent $\chi(\boldsymbol{q},\omega)$, $1/T_1$ is known to be expressed from Eq. (1) as[15]

$$\frac{1}{T_1} = \frac{\sqrt{2\pi}(\gamma_N A_{iso}/z')^2 p_{ord}^2}{3\omega_{fl}}, \tag{2}$$

where ω_{fl} is the local-moment fluctuation rate, p_{ord} is the ordered moment, and z' is the number of Ce ions around the nuclear sites. ω_{fl} is given by two major processes, that is, $\omega_{fl} = \omega_{ex} + \omega_{cf}$. The ω_{ex} represents a fluctuation process caused by the intersite RKKY exchange interaction J_{ex}, which is denoted as $(\hbar\omega_{ex})^2 = (2z/3\hbar^2)(J_{ex}p_{ord})^2$, with z being the number of nearest-neighboring Ce ions. On the other hand, ω_{cf} is due to the spin-exchange interaction with conduction electrons and is written as $\hbar\omega_{cf} \approx (\pi/\hbar)(J_{cf}\rho)^2 k_B T$, where J_{cf} is the intrasite spin-exchange coupling between the Ce

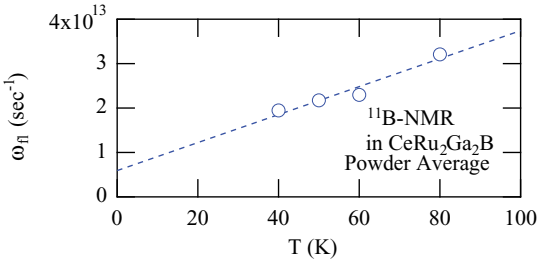

FIG. 11. (Color online) (a) Temperature dependence of powder averaged $\omega_{\rm fl} \propto T_1$ by ^{11}B NMR in $CeRu_2Ga_2B$.

local moments and conduction electrons. $\omega_{\rm cf}$ thus provides a T-linear dependence for T_1. Assuming the ordered moment is 1.3 μ_B/Ce, the temperature dependence of $\omega_{\rm fl}$ derived from the powder averaged $1/T_1$ for ^{11}B is plotted as shown in Fig. 11, which can be fitted by $\alpha + \beta T$. The obtained $\alpha = 6 \times 10^{12}$ s^{-1} yields $|J_{\rm ex}|/k_B \sim 20$ K, which is the same order as T_C. The $\beta = 3 \times 10^{11}$ $s^{-1}\,K^{-1}$ gives an apparent estimate of $J_{\rm cf}\rho \sim 0.85$, which is larger than typical for heavy fermion systems. For example, in the heavy fermion systems such as $CeCu_2Si_2$, UBe_{13}, and $CeCoIn_5$, $J_{\rm cf}\rho$ ranges in value from 0.1 to 0.2.[16]

This apparent value of $J_{\rm cf}\rho$ may be useful for a systematic comparison in the $LnRu_2X_2X'$ (Ln = La, Ce, Pr, . . .; X = Al, Ga; X' = B, C) series. For example, systematic NMR investigations of $LnRh_3B_2$[17] may suggest that the strong hybridization of f electrons with conduction electrons causes a small ordered moment of ∼0.38 μ_B/Ce as $J_{\rm cf}\rho$ increases. Indeed, such a Korringa behavior, that is, a T-independent $(T_1T)^{-1}$ corresponding to strong hybridization in the high temperature region, is seen in the highest T_C of Ce-based FM materials $CeRh_3B_2$ with $T_C \sim 112$ K.[17,18] Moreover, in $CeRh_3B_2$, by applying pressure (P), a decrease of T_C is observed around $J_{\rm cf} \sim 1.1J_0$ ($P \sim 3.5$ GPa) and the disappearance of T_C around $J_{\rm cf} \sim 1.2J_0$ ($P \sim 7$ GPa), where J_0 is the value of $J_{\rm cf}$ under ambient pressure.[19] Thus, the shift of the apparent $J_{\rm cf}\rho$ by pressures or substitutions may become an indicator of proximity to FM quantum criticality.

As a last remark, in the ordered state below T_C, $1/^{69}T_1$ decreases steeply as temperature decreases, and follows the power law T^5, as shown in Fig. 9(a). In a FM ordered state of localized moments, a two-magnon Raman or three-magnon process usually governs the relaxation mechanism, which yields T^2 or $T^{7/2}$ behavior, respectively.[20] In this case, the steeper exponent of 5 may suggest that the relaxation mechanism is not governed by such a simple magnon process. Perhaps the strong Ising-type anisotropy and the polarization of the conduction bands in the FM ordered state may have to be considered to explain the T^5 behavior for this system.

IV. SUMMARY

^{11}B and ^{69,71}Ga NMR measurements have been performed on the Ce-based FM system $CeRu_2Ga_2B$ with $T_C(H_0 = 0) = 16.3$ K. The values of ν_Q for ^{11}B and ^{69}Ga are estimated from the NMR spectra under applied fields. Isotropic hyperfine coupling constants are determined for ^{11}B and ^{69}Ga in the paramagnetic state through Knight shift measurements. The zero applied field NMR spectra for ^{69,71}Ga are successfully obtained, which gives precise values of the internal field on the Ga sites. At the same time, somewhat larger values of ν_Q for ^{69}Ga are obtained, which may suggest magnetovolume expansion without symmetry lowering. Nuclear spin-lattice relaxation $1/T_1$ measurements reveal the Ising-type anisotropy for the FM spin fluctuations. The absolute values and temperature dependence of $1/T_1$ suggest a well-localized 4f picture for this system: The local moments of Ce^{3+} fluctuate as a result of FM intersite coupling ($J_{\rm RKKY} \sim 20$ K) above T_C and individually fluctuate due to intrasite coupling $J_{\rm cf}$ well above T_C. Thus, this NMR study has microscopically characterized the static and dynamic magnetic responses in the new Ce-based ferromagnet $CeRu_2Ga_2B$ and provides the basis to understand this new series of $CeRu_2X_2X'$ compounds.

ACKNOWLEDGMENTS

We would like to thank Y. Haga, H. Chudo, and H. Yasuoka for stimulating discussions and suggestions. A part of this work was supported by a Grant-in-Aid for Scientific Research on Innovative Areas Heavy Electrons (No. 20102006 and No. 20102007) by the MEXT of Japan. This research was also partially supported by the REIMEI Research Program of JAEA. Work at Los Alamos National Laboratory was performed under the auspices of the US Department of Energy, Office of Basic Energy Sciences, Division of Materials Sciences and Engineering, PECASE funding from the US DOE, OBES, Division of Material Science and Engineering, and funded in part by the Los Alamos Laboratory Directed Research and Development program.

*sakai.hironori@jaea.go.jp

[1] S. Kambe, H. Sakai, Y. Tokunaga, T. Fujimoto, R. E. Walstedt, S. Ikeda, D. Aoki, Y. Homma, Y. Haga, Y. Shiokawa *et al.*, Phys. Rev. B **75**, 140509(R) (2007).

[2] S.-H. Baek, H. Sakai, E. D. Bauer, J. N. Mitchell, J. A. Kennison, F. Ronning, and J. D. Thompson, Phys. Rev. Lett. **105**, 217002 (2010).

[3] H. Sakai, S. Kambe, Y. Tokunaga, Y. Haga, S.-H. Baek, F. Ronning, E. D. Bauer, and J. D. Thompson, Mater. Res. Soc. Symp. Proc. **1264**, 69 (2010).

[4] R. E. Baumbach, T. Shang, M. Torrez, F. Ronning, J. D. Thompson, and E. D. Bauer, J. Phys.: Condens. Matter **24**, 285702 (2012).

[5] R. E. Baumbach, H. Chudo, H. Yasuoka, F. Ronning, E. D. Bauer, and J. D. Thompson, Phys. Rev. B **85**, 094422 (2012).

[6] E. Matsuoka, Y. Tomiyama, H. Sugawara, T. Sakurai, and H. Ohta, J. Phys. Soc. Jpn. **81**, 043704 (2012).

[7] H. Matsuno, H. Nohara, H. Kotegawa, E. Matsuoka, Y. Tomiyama, H. Sugawara, H. Harima, and H. Tou, J. Phys. Soc. Jpn. **81**, 073705 (2012).

[8] R. E. Baumbach, X. Lu, F. Ronning, J. D. Thompson, and E. D. Bauer, J. Phys.: Condens. Matter **24**, 325601 (2012).

[9] J. V. Zaikina, Y.-J. Jo, and S. E. Latturner, Inorg. Chem **49**, 2773 (2010).

[10]H. F. Braun and J. L. Jorda, Physica B+C **135**, 72 (1985).
[11]C. Petrovic, P. G. Pagliuso, M. F. Hundley, R. Movshovich, J. L. Sarrao, J. D. Thompson, Z. Fisk, and P. Monthoux, J. Phys.: Condens. Matter **13**, L337 (2001).
[12]T. Moriya, J. Phys. Soc. Jpn. **18**, 516 (1963).
[13]T. Moriya, J. Magn. Magn. Mater. **100**, 261 (1991).
[14]Y. Ihara, T. Hattori, K. Ishida, Y. Nakai, E. Osaki, K. Deguchi, N. K. Sato, and I. Satoh, Phys. Rev. Lett. **105**, 206403 (2010).
[15]T. Moriya, Prog. Theor. Phys. **16**, 23,641 (1956).
[16]Y. feng Yang, Z. Fisk, H.-O. Lee, J. D. Thompson, and D. Pines, Nature (London) **454**, 611 (2008).
[17]Y. Kishimoto, Y. Kawasaki, and T. Ohno, J. Phys. Soc. Jpn. **73**, 1970 (2004).
[18]Y. Kitaoka, Y. Kishimoto, K. Asayama, T. Kohara, K. Takeda, R. Vijayaraghavan, S. K. Malik, S. K. Dhar, and D. Rambabu, J. Magn. Magn. Mater. **52**, 449 (1985).
[19]A. L. Cornelius and J. S. Schilling, Phys. Rev. B **49**, 3955 (1994).
[20]D. Beeman and P. Pincus, Phys. Rev. **166**, 359 (1968).